NUMERICAL DEVELOPMENT OF A FLUTTER ACTIVE CONTROL SYSTEM BASED ON PRESSURE FEEDBACK

T. F. G. Costa, E. M. Belo
School of Engineering of Sao Carlos – University of Sao Paulo, Brazil

Keywords: *flutter, aeroelasticity, aeroservoelasticity, flutter suppression*

Abstract

The purpose of this work is to show, by simulation, the development of a flutter suppression active control system using pressure sensors in strategic points on an aircraft wing surface.

The aeroelastic response is obtained in time domain as a result of the numeric integration of the motion equations of the structure. These equations represent the wing structural dynamics excited by aerodynamics non-stationary loads. The structure is modeled by Finite Element Method (using NASTRAN®), and the aerodynamics is modeled using non-stationary vortex-lattice method (using FORTRAN90 language). The coupling of both models meshes is done using a surface spline method

Comparing aeroelastic response for cases with control system on and off, it is possible to conclude that a system SISO (single-input, single-output) has enough efficiency. The best position for the pressure sensor, and the best controller gain were also determined.

1 Introduction

Flutter is an aeroelastic phenomenon characterized by an unstable coupling of a flexible structure and a non-stationary aerodynamic flow [11]. Frequently, this instability leads to structure fail, and must be avoided.

With constant aircraft optimization, structures tend to be lighter, commonly leading to more flexibility [11]. When changes on the wing structure or aerodynamics are not viable to avoid flutter (passive counter-measures), the use of automatic control systems becomes a good option. In the 60's, Cole et al. [12] affirm that such systems would soon be applied.

The intention of this work is to develop a numeric model to verify the efficiency of automatic controllers based on simple control laws. The design of the suggested control system will be developed as a numeric model of a finite flexible wing and implemented computationally. With this model and the pressure over the wing surface read in certain points and fedback to the control system, changes of the control surface angle on the trailing edge are determined.

The attempt to use a simple control system, with a unique pressure sensor shows the viability of implementing this kind of system in real aircrafts. Flutter experiments were already performed to demonstrate flutter suppression with simple control laws [13]. This numerical model allows studying flutter occurrence and controlling it before the aircraft or the experiment complete development.

This work shows the analysis for speeds varying from critical speed to about 20% above. Speeds higher than that were not tested since it is supposed improbable that the structure of the tested wing could support the loads (even static ones). As part of the conclusion, a study of the efficiency of the gain and the best position for the pressure sensor were presented.

2 The Numerical Model

2.1 The Wing Simulated

A real wing with experimental modal analysis data available [3] was taken as reference for this

entire work. The wing is rectangular with a 2.980m span and 0.220m chord, with no sweep and no dihedral. Its structure is composed by a Styrofoam core, unidirectional carbon fiber span and a bi-directional kevlar shell [2]. The airfoil is a Selig S1223 [2] [10]. A material properties table and details of the finite element model used to represent wing structure can be found in reference [4].

The mathematical model to represent this wing is composed by

- A finite element structural mesh for modal analysis, adjusted to obtain the same natural frequencies as the experiment [3] [4];

- A vortex-lattice mesh for non-stationary aerodynamic analysis using a camber line that results in the same C_L and C_M as the Selig S1223 airfoil at 5º of angle of attack (angle used to perform the simulations) [10]. The use of a camber line is important to guarantee real magnitudes of lift and pitching moment, increasing solution accuracy.

2.2 Finite Element Structural Model

The matrix equation used to describe the harmonic oscillatory motion, not excited and not damped, of a flexible linear structure [1] is given by:

$$[M]\{\ddot{x}(t)\}+[K]\{x(t)\}=0 \qquad (1)$$

where: $[M]$ = Mass matrix;

$[K]$ = Elastic matrix;

$\{x(t)\}$ = Displacements vector, as function of time.

In case of a structure excited by forces $\{F\}$ dependant on structure geometry, structure displacement velocity and time, equation (1) can be rewritten as:

$$[M]\{\ddot{x}(t)\}+[K]\{x(t)\}=\{F(t,x(t),\dot{x}(t))\} \qquad (2)$$

However, finite element models usually have a large number of degrees of freedom, what leads to a high order of $[M]$ and $[K]$.

To simplify the model order the structure harmonic motion can be described as a linear composition of the natural modes. It is known that only the low frequencies are relevant. So, equation (2) becomes:

$$\{\ddot{\eta}(t)\}+[\omega^2]\{\eta(t)\}=[\hat{\Phi}]^T\{F(t,x(t),\dot{x}(t))\} \qquad (3)$$

where: $[\omega^2]$ = Matrix with the natural frequencies in the diagonal;

$\{\eta(t)\}$ = Modal displacement vector, as function of time.

$[\hat{\Phi}]^T$ = Matrix with one natural mode per row, which is the transposed of the classic eigenvalue solution $[\Phi]$, normalized with respect to the inertia matrix according to:

$$[\hat{\Phi}]=[\Phi][M]^{-1/2} \qquad (4)$$

The transformation between $\{x(t)\}$ and $\{\eta(t)\}$ is:

$$\{x(t)\}=[\hat{\Phi}]\{\eta(t)\} \qquad (5)$$

$$\{\ddot{x}(t)\}=[\hat{\Phi}]\{\ddot{\eta}(t)\} \qquad (6)$$

2.3 Vortex-Lattice Aerodynamic Model

The vortex-lattice method consists in divide the wing platform in several panels. Each panel has a closed vortex ring, respecting Helmholtz theorem [5].

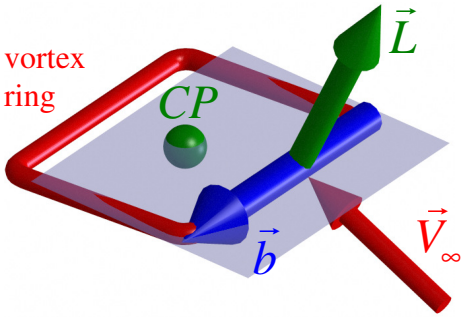

Fig. 1 – The vortex-lattice panels, vortex ring and reference vectors.

where: $\vec{V}_\infty$ = Free flow velocity;

$\vec{b}$ = Panel span;

$\vec{L}$ = Lift;

CP = Control point.

The lift of the wing is a composition of the lift of all panels. The equation used to calculate

panel lift is obtained from Bernoulli equation [5] and prepared to be used in an iterative process [4] [6] as:

$$L=\left[\rho\Gamma(t)\left(\vec{V}_{\infty}\times\vec{b}\right)+S_{pn}\rho\frac{\Gamma(t)-\Gamma(t-\Delta t)}{\Delta t}\vec{N}_{pn}\right]\cdot\vec{N}_{w} \qquad (7)$$

where: L = Lift as a scalar number;

$\Gamma(t)$ = Vortex ring intensity (vorticity), as function of time;

S_{pn} = Panel area;

$\vec{N}_{pn}$ = Unitary vector normal to panel plane;

$\vec{N}_{w}$ = Unitary vector normal to wing plane.

In order to solve the aerodynamic model, and find the components of all aerodynamic forces perpendicular to the wing, it is necessary to determine the vorticity distribution over the wing.

In each control point of the aerodynamic model, the velocity induced by all vortex ring can be found imposing that the velocity component perpendicular to the wing should be zero to guarantee that there is no airflow crossing wing surface. The following equation is obtained:

$$\sum_{j=1}^{n_{wing}}\vec{N}_{i}\cdot\vec{V}_{ij}\Gamma_{j}=-\vec{N}_{i}\cdot\left(\vec{V}_{\infty}+\vec{V}_{pc_i}+\sum_{k=1}^{n_{wake}}V_{ik}\right) \qquad (8)$$

where: $\vec{N}_{i}$ = Unitary vector normal to panel i;

Γ_{i} = Vortex ring intensity of panel i;

$\vec{V}_{pc_i}$ = Control point velocity due to flexible motion of the structure;

V_{ij} = Induced velocity of o wing panel j on the control point of panel i;

V_{ik} = Induced velocity of a wake panel k on the control point of panel i;

n_{wing} = Number of panels in wing mesh;

n_{wake} = Number of panels in wake mesh;

Using equation (8) for all wing panels, a linear system is obtained. Its solution is the vorticity distribution.

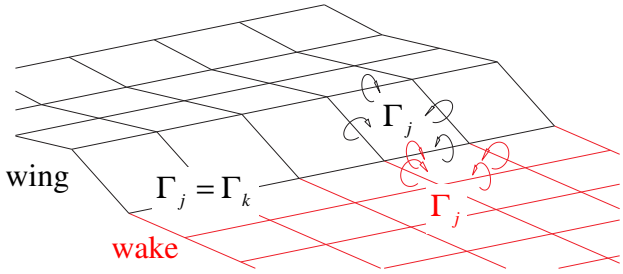

Fig. 2 – Kutta condition

Kutta condition states that the intensity of the vortex at the trailing edge should be zero [7]. To satisfy Kutta condition each first panel of the wake must have the same intensity of the wing panel in front of it (Fig. 2).

The induced velocities V_{ij} and V_{ik} are calculated according to the Biot-Savart law [7] [5] (Fig. 3 and equation (9)).

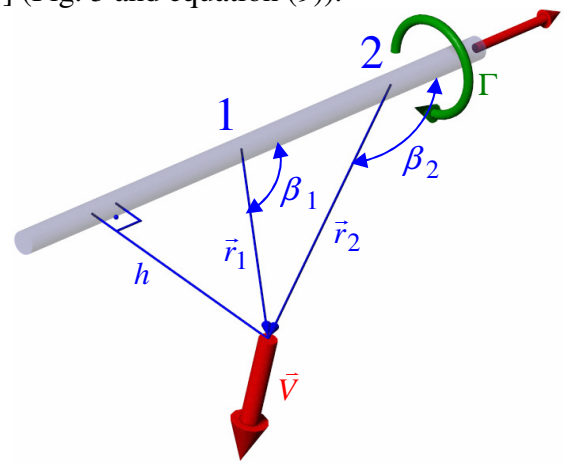

Fig. 3 – Biot-Savrat law, simplified to a straight vortex segment [5].

$$\vec{V}=\frac{\Gamma}{4\pi}\frac{\vec{r}_1\times\vec{r}_2}{\left|\vec{r}_1\times\vec{r}_2\right|^2}\left(\frac{\vec{r}}{|\vec{r}|}-\frac{\vec{r}_2}{|\vec{r}_2|}\right)\cdot\left(\vec{r}_1-\vec{r}_2\right) \qquad (9)$$

The induced velocities V_{ij} and V_{ik} for the entire ring are just the sum of the induced velocities of each segment of the ring calculated with equation (9).

2.4 Surface Spline Method for Coupling Meshes

The coupling of aerodynamic and structural models is important, since the forces obtained in the aerodynamic mesh (equation (7)) should be used in equation (3), that is written in structural mesh. At the same time, the motion obtained on the solution of equation (3) should be

transported to aerodynamic mesh to solve the load distribution (equations (7), (8) and (9)).

The surface spline interpolation method [8] is very useful in this case. Interpolating the structural mesh to find the same mode shapes in aerodynamic mesh for control points and for vortex ring vertices, it is possible to do the following conversions [4] [6]:

$$\{\bar{z}_a\} = [G]\{\bar{z}_s\} \quad (10)$$

$$\{\dot{\bar{z}}_a\} = [G]\{\dot{\bar{z}}_s\} \quad (11)$$

$$\{F_s\} = [G]^T \{F_a\} \quad (12)$$

where: $\{\bar{z}\}$ = Vector of nodal displacements normal to the wing plane;

$\{\dot{\bar{z}}\}$ = Vector of nodal velocities normal to the wing plane;

$\{F\}$ = Vector of forces normal do the wing plane;

s = subscript relative to structural mesh;

a = subscript relative to aerodynamic mesh;

$[G]$ = transformation matrix. The procedure to determine this matrix in found in references [8], [4] and [6];

Since the modal matrix is a matrix composed of several vectors of structural displacements, equation (3) can be rewritten as:

$$\{\ddot{\eta}(t)\} + [\omega^2]\{\eta(t)\} = \left[\hat{\Phi}_a\right]^T \{F_a(t, x(t), \dot{x}(t))\} \quad (13)$$

where: $\left\{\hat{\Phi}_a\right\}^T$ = transposed of the modal matrix written in coordinates of the control points of the aerodynamic mesh.

2.5 Integration Method

Finally, equation (13) can describe the physics of the aeroelastic model, relating aerodynamic forces and inertia forces. However, it can't be solved analytically, since the vector $\{F_a\}$, containing the forces, can't be described as a mathematical equation. It is result of all the procedure described in section 2.3.

A numerical integration is used to solve equation (13). The predictor-corrector method was used in form PECLE, described by Lambert [9], using the collection of methods Adams-Bashforth for predictor step and Adams-Moulton for corrector step [9] [4] [6]. This method is used solve first order differential equations. Therefore equation (13) should reduced to:

$$\begin{aligned} \dot{X}_1 &= X_2 \\ \dot{X}_2 &= \left[\hat{\Phi}_a\right]^T \{F_a(t, x(t), \dot{x}(t))\} - [\omega^2] X_1 \end{aligned} \quad (14)$$

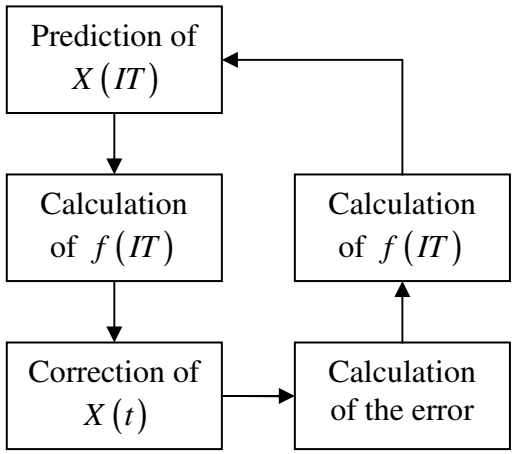

Fig. 4 – Predictor-corrector in form PECLE

where: IT = Iteration number;

X = Left hand side of system equation (14);

f = Right hand side of system equation (14).

2.6 Control System

As presented on section 2.5, it is necessary to use a numerical method to solve the model without any controller. The use of a feedback controller increases the complexity of the model.

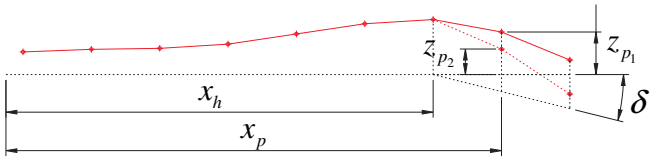

Fig. 5 – Control surface deflection.

Since the integration process is iterative and based on time step, the control model can be implemented just by applying the control law in intermediary steps of the solving process. At the same moment as aerodynamic mesh is refreshed, movement in certain panels represents the control surface deflection (Fig. 5).

$$z_{p_2} = z_{p_1} - \left(x_p - x_h\right) tg\,\delta \qquad (15)$$

where: p = Sub-index indicating point being displaced;

h = Sub-index indicating control surface hinge position;

δ = Control surface deflection.

The main objective of the control system proposed is to provide an artificial damping to avoid flutter phenomenon. For that, the control law adopted was a deflection on control surface proportional to the variation of the pressure over wing surface, read by a sensor positioned in a convenient panel. (Fig. 6)

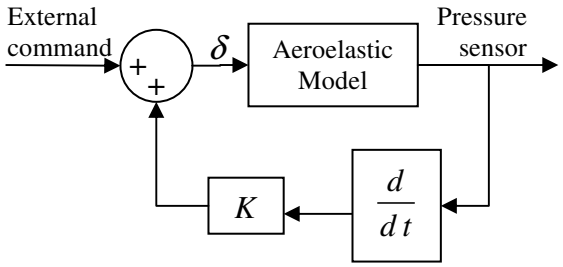

Fig. 6 – Block diagram for the controlled model.

Disregarding the external command the expression for the control surface deflection is:

$$\delta = K\,\frac{P\left(t+\Delta t\right) - P\left(t+\Delta t\right)}{\Delta t} \qquad (16)$$

where: K = Gain proportional to the pressure derivative with respect to time;

$P\left(t\right)$ = Pressure read by the sensor in time t;

Δt = Step time used in numerical integration.

3 Simulations and Results

All simulations in this work kept the following parameters constant:

- air density: 1.225kg/m^3
- wing airfoil as Fig. 7
- wing angle of attack: 5º
- wake truncation length: 4.0m
- simulation total time: 0.300s
- number of panels chordwise: 8
- number of panels spanwise: 13
- integration step according to equation (17) with V_∞ in m/s
- wake displacement depends only on free flow speed.

$$\Delta t = \frac{0.006}{V_\infty} \qquad (17)$$

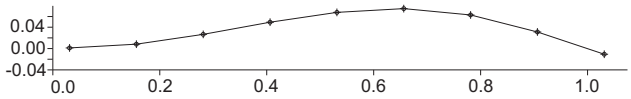

Fig. 7 – Camber line representative of Selig S1223 profile at 5º angle of attack: C_L = 1.5094 and C_M = -0.290

3.1 Flutter Critical Speed

To find the flutter critical speed, several simulations were performed, and the aeroelastic responses were compared. It was assumed that the critical speed is between the first speed with divergent behavior and the last with convergent behavior. Fig. 8 to Fig. 11 show that flutter critical speed is about 70m/s.

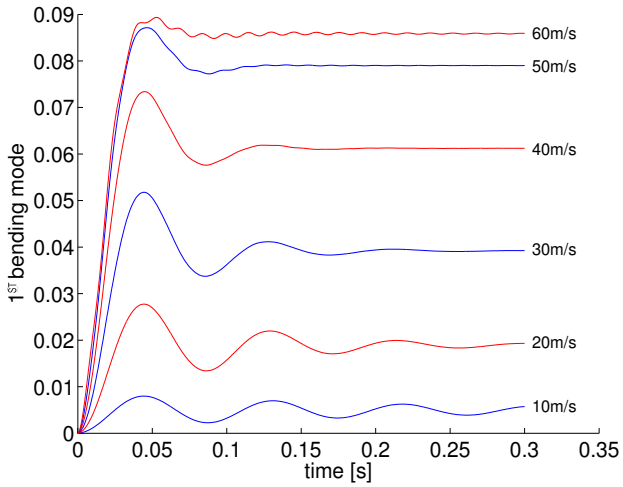

Fig. 8 – Behavior of 1st bending mode for speeds until 60.0m/s.

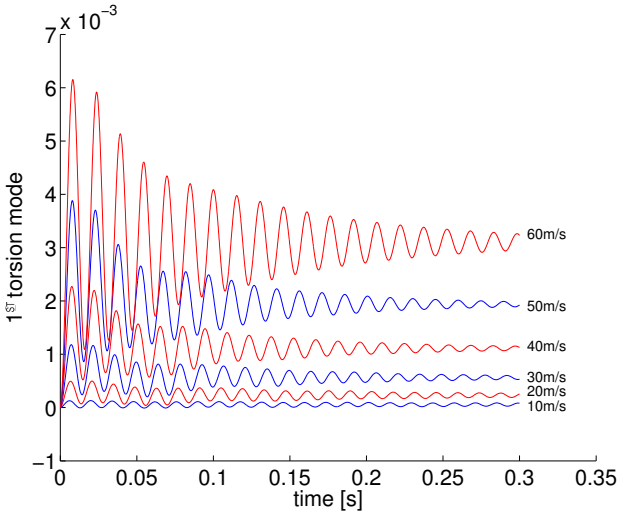

Fig. 9 – Behavior of 1st torsion mode for speeds until 60.0m/s.

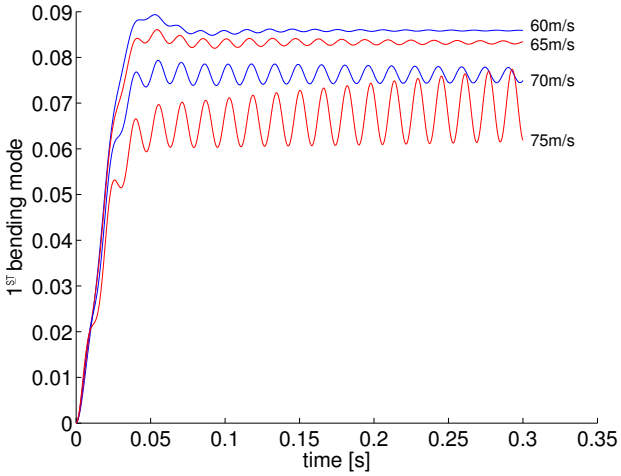

Fig. 10 – Behavior of 1st bending mode for speeds above 60.0m/s.

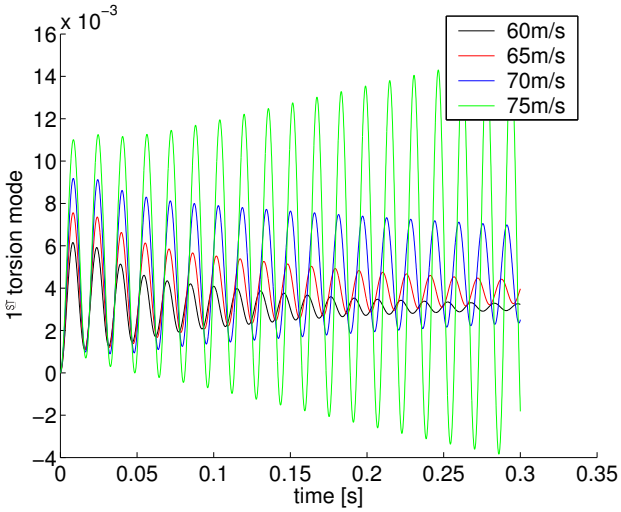

Fig. 11 – Behavior of 1st torsion mode for speeds above 60.0m/s.

3.2 Flutter Suppression Control System

An unique pressure sensor is used in each simulation. Four positions (panels) were tested, as indicate Fig. 12

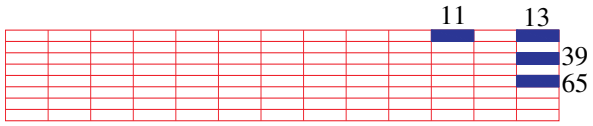

Fig. 12 – Panels were sensors were tested. Panels are numbered sequentially from wing root and leading edge to wing tip and trailing edge.

Panel 13 was the first to be verified. It is the first panel along the chord (where the difference in pressure between the upper and lower side of the wing is maximum) and the last panel in span (where the displacement due to bending and torsion is maximum).

After panels 39, 65 and 11 were tested to verify the difference in efficiency when compared to panel 13.

To compare the damping obtained in each case, the Fourier Transforming was applied to aeroelastic response, presenting a peak in dominant frequency. The damping of the system is lower as much the peak in frequency response plots is higher. The comparison of all peak sizes leads to Fig. 13 and Fig. 14, where the "peak ratio" is shown. Peak ratio is the value of the peak for each case divided by the value of the peak in the not controlled case. For all cases in Fig. 13 and Fig. 14 the controller was turned on after 0.05s.

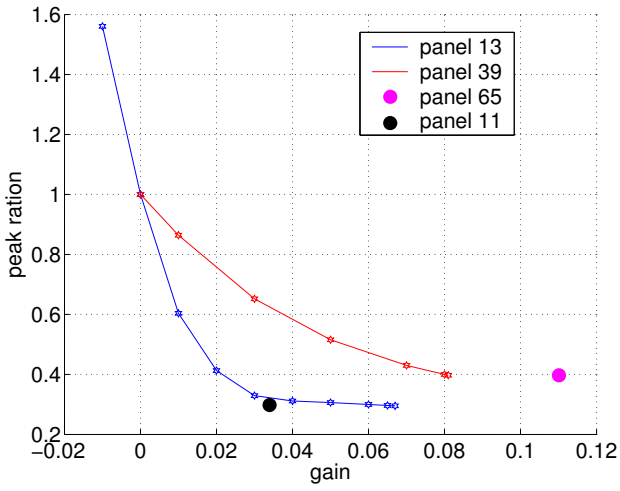

Fig. 13 – Peak ratio for 1st bending mode

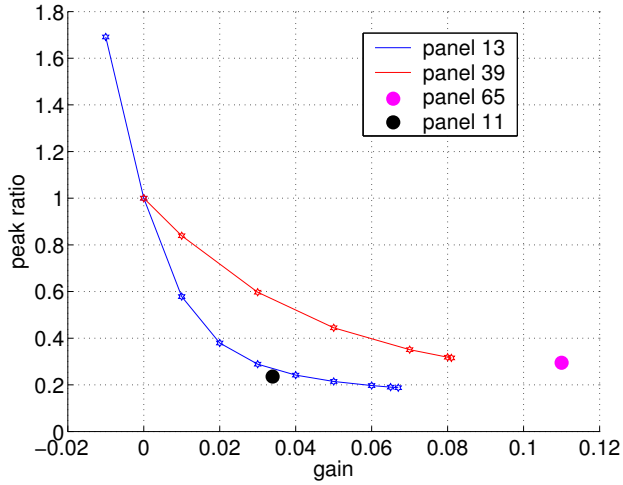

Fig. 14 – Peak ratio for 1st torsion mode.

In Fig. 13 and Fig. 14 the maximum gain value for panels 13 and 39 were limited by divergence problems. High values of gain lead to numeric instability. For panel 11 and 65 only the maximum gain was plotted. The existence of a numeric noise can be verified in Fig. 15 and probably is this noise that causes instability and divergence for high values of gain.

The responses in frequency domain are shown from Fig. 16 to Fig. 19. For panel 13 an extra case was analysed, turning on the controller at instant 0.0008s.

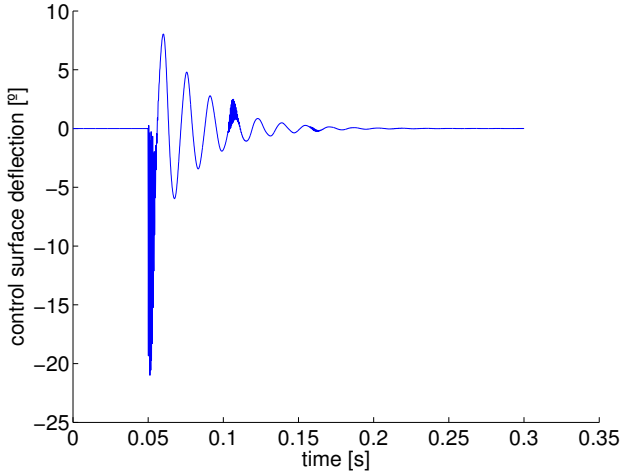

Fig. 15 – Control surface deflection angle for case with sensor in panel 13, gain = 0.067 and speed = 75m/s.

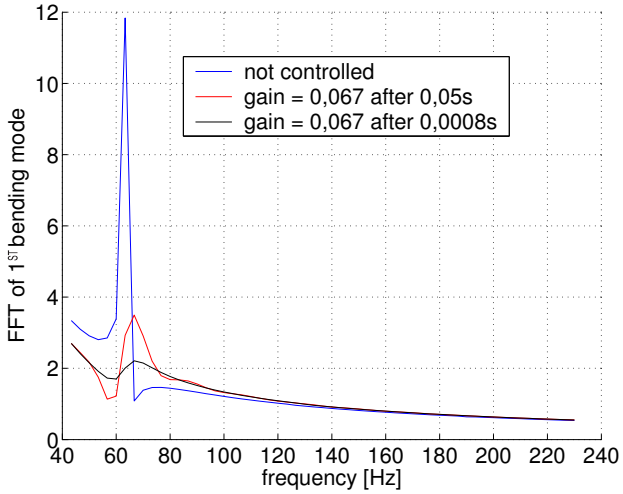

Fig. 16 – Response in frequency domain for 1st bending mode, sensor in pane 13 and speed = 75 m/s

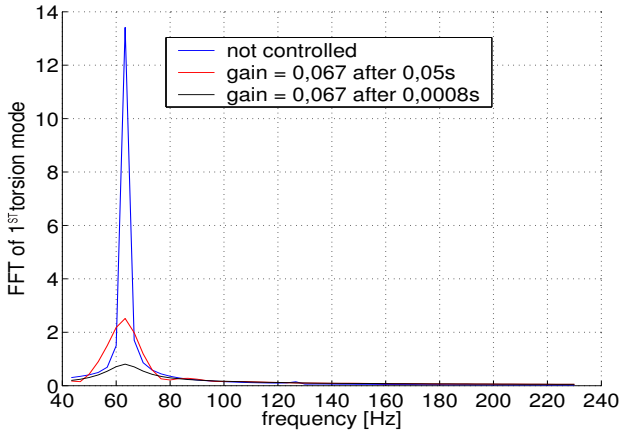

Fig. 17 – Response in frequency domain for 1st torsion mode, sensor in pane 13 and speed = 75 m/s

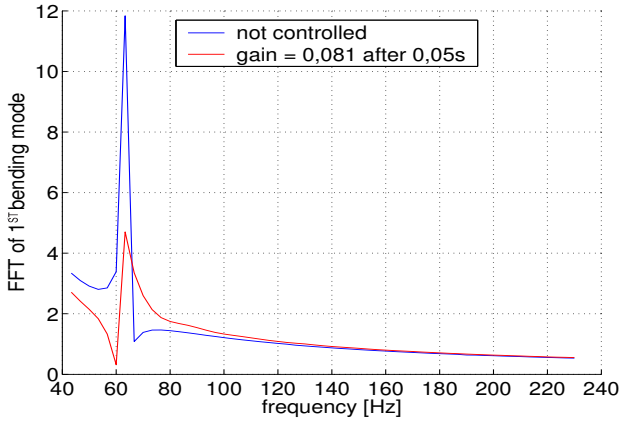

Fig. 18 – Response in frequency domain for 1st bending mode, sensor in pane 39 and speed = 75 m/s

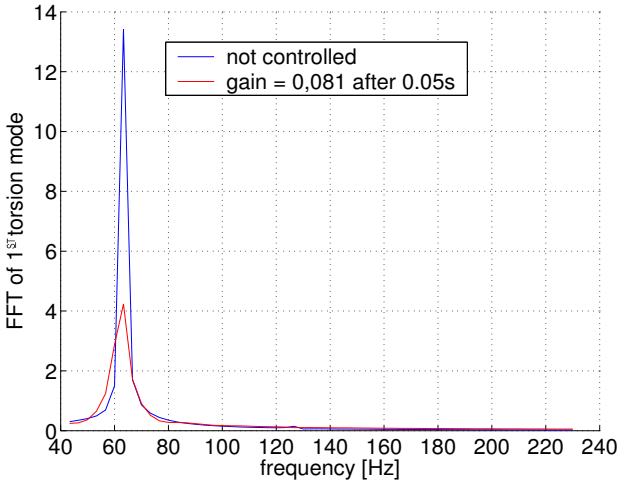

Fig. 19 – Response in frequency domain for 1st torsion mode, sensor in pane 39 and speed = 75 m/s

In order to help visualization, the aeroelastic response in time is shown from Fig. 20 to Fig. 23. One can note the effect of the feedback controller in damping of the system is very significant.

To finish this study and verify the reliability of this controller, simulations extrapolating flutter critical speed were done and even for these cases the controller shows to be effective (Fig. 24 and Fig. 25).

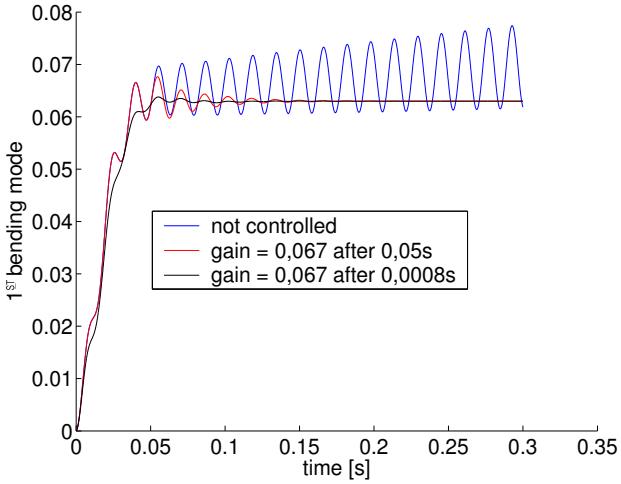

Fig. 20 – Behavior of 1st bending mode for sensor in panel 13, and speed = 75 m/s.

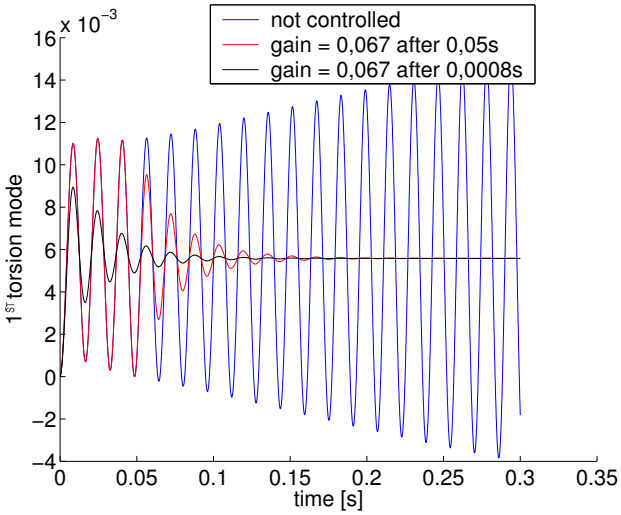

Fig. 21 – Behavior of 1st bending mode for sensor in panel 13, and speed = 75 m/s.

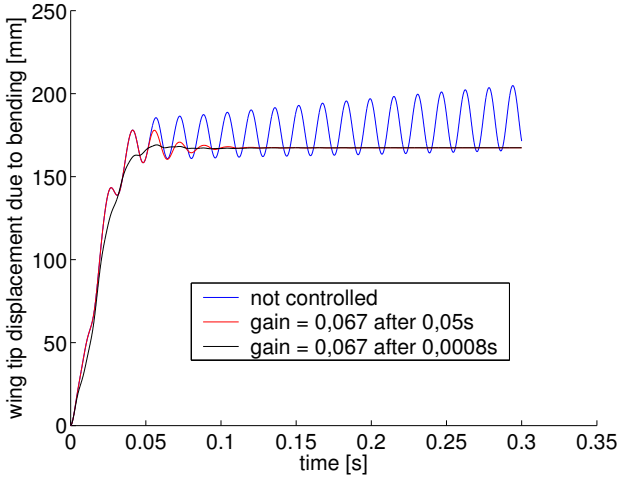

Fig. 22 – Wing tip displacement due bending for sensor in panel 13, and speed = 75 m/s.

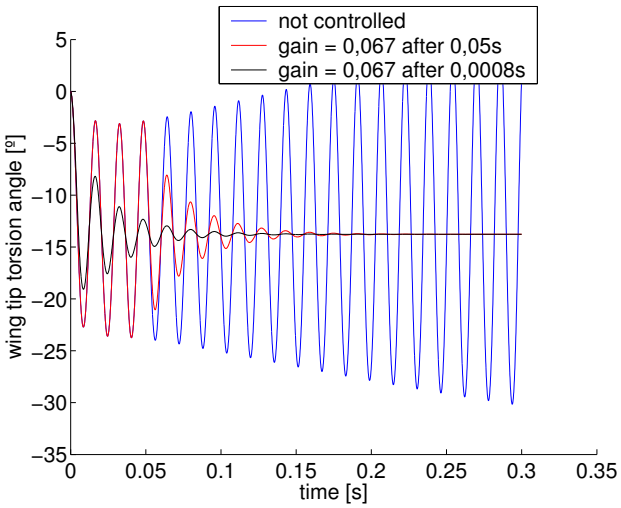

Fig. 23 – Wing tip torsion for sensor in panel 13, and speed = 75 m/s.

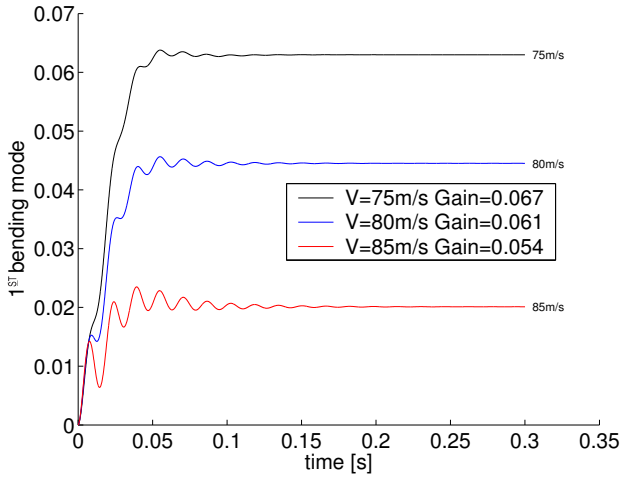

Fig. 24 – Behavior of 1st bending mode for sensor in panel 13, and speeds from 75 m/s to 85m/s.

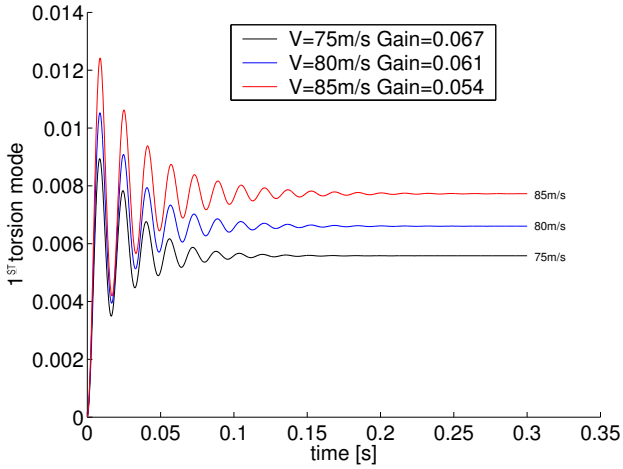

Fig. 25 – Behavior of 1st torsion mode for sensor in panel 13, and speeds from 75 m/s to 85m/s.

4 Conclusions

The numeric model of a control system to suppress flutter on a wing was developed. It shows to be very efficient, even for a simple control law.

A numeric instability occurred to high values of gain, leading to divergence in solution iterative process. Probably, a low frequency filter applied to the system could solve the problem.

The results presented may encourage future research and use of this type of system on aeronautic industry, to prevent flutter and increase the life of structures and components of aircrafts, reducing the oscillation and harmonic motion of the structure (reduce the number of cycles).

The aeroelastic model herein developed can be easily adapted to simulate flutter in morphing wings and may encourage future research in this area.

In addition, the system based on pressure feedback may become an alternative to those developed until now, using accelerometers. Yet, it could be useful, in systems where it is necessary to predict stall and observe the pressure load behavior over the wing in flight (cases where pressure sensor are already been used).

References

[1] Craig Jr., R. R. *Structural Dynamics: an Introduction to Computer Methods.* John Wiley & Sons, Inc, 1981.

[2] Equipe EESC-USP de AeroDesign (2002). *Technical Report – AeroDesign East 2002*. Titusville, 2002.

[3] Marques, F. D.; Varoto, P. S.; Benini, G. R.; Oliveira, L. P. R. An investigation on the modal characteristics of an aircraft wing structure. In: Espíndola, J. J. et al. ads., *Dynamic Problems of Mechanics.* Rio de Janeiro. ABCM. pp. 465-469, 2001.

[4] Costa, T. F. G. *Numeric study of a wing with flutter active control by feedback of the pressure measured in one point.* 122pp. Dissertation (M. Sc.) – Engineering School of Sao Carlos, University of Sao Paulo, Sao Carlos, 2007.

[5] Katz, J.; Plotkin, A. *Low-Speed Aerodynamics.* 2ªed Cambridge University Press, 2001.

[6] Benini, G. R. *Modelo Numérico para Simulação da Resposta Aeroelástica de Asas Fixas. Dissertação (Mestrado)* – Escola de Engenharia de São Carlos, Universidade de São Paulo, 2001.

[7] Anderson, J. D. *Fundamentals of aerodynamics*. 2ªed McGraw-Hill, Inc, 1991

[8] Harder, R. L.; Desmarais, R. N. *Interpolation Using Surface Splines*. Journal of Aircraft; Vol. 9, nº 2, p.189-191, 1972

[9] Lambert, J. D. *Numerical Methods for Ordinary Differential Systems: The Initial Value Problem.* John Wiley & Sons, Inc, 1991

[10] Selig M. UIUC Low-Speed Airfoil Tests. http://www.ae.uiuc.edu/mselig/pub/LSATs/AppendedFiles_vol1/LIFT01.TXT (30 march, 2006)

[11] Bisplinghoff, R. L.; Ashley, H. (2002); *Principles of Aeroelasticity*. Dover Publications, Inc., Mineola – NY

[12] Cole, S. R.; Noll, T. E.; Perry, B. (2003); Transonic Dynamics Tunnel Aeroelastic Testing in Support of Aircraft Development. *Journal of Aircraft*; Vol. 40, nº 5, p.820-831.

[13] Waszak, M. R.; Srinathkumar, S. (1995); Flutter Suppression for the Active Flexible Wing: A

Classical Design. *Journal of Aircraft*; Vol. 32, nº 1, p.61-67

[14] Bartels, R. E.; Schuster, D. M. (2000); Comparison of Two Navier-Stokes Methods with Benchmark Active Control Technology Experiments. *Journal of Guidance*, Control and Dynamics; Vol. 23, nº 6, p.1094-1099.

Copyright Statement